Computational Materials Science 97 (2015) 94–101

Contents lists available at ScienceDirect

Computational Materials Science

journal homepage: www.elsevier.com/locate/commatsci

Numerical analysis of elastic and elastoplastic behavior of interpenetrating phase composites

Fan Xie, Zixing Lu *, Zeshuai Yuan

Institute of Solid Mechanics, Beihang University, Beijing 100191, China

ARTICLE INFO

Article history:
Received 5 June 2014
Received in revised form 8 October 2014
Accepted 12 October 2014

Keywords:
Interpenetrating phase composite (IPC)
Phase field method
3D random model
Finite element method (FEM)
Elastoplastic behavior

ABSTRACT

A routine is compiled to describe the spatial distributions of interpenetrating phases by solving the phase field equation. And a 3D random finite element (FE) model based on the phase field method is presented which can characterize the realistic microstructure of the interpenetrating phase composite (IPC) for the first time. Compared with the previous models, the present model is easier to generate at a low cost. The statistical criterion has been employed to determine the critical size of the 3D random FE model. The sample capacity has also been discussed. In addition, the cross-cubic model and the tetrakaidecahedron model are also conducted by finite element method (FEM) for comparison. Furthermore, the Young's modulus and elastoplastic properties of IPC are predicted by FE models and theoretical methods, and the results of the 3D random FE model accord well with experimental data.

1. Introduction

The interpenetrating phase composites (IPCs), also called co-continuous or bicontinuous composites are advanced engineering materials which consist of two pure phase materials. Each phase contributes its own properties to the multifunctional characteristics of the whole structure. If either of the two phases were removed from such a composite, the remaining constituent would form an open-cell foam, which alone can still bear loads. As constituents of composite are interconnected in 3D space and twine in all directions, the interface-to-volume (interface denotes interface/surface between two phases) ratio is pretty high. Hence, IPCs possess unique mechanical properties and physical properties which are different from and even superior to the conventional fiber or particle-reinforced materials. There are various IPCs composed of different constituents, for example ceramic-metal [1], interpenetrating polymer network [2] and metal/ceramic foam base IPC [3–6].

It is a challenge to study the mechanical properties of IPCs for their complicated microstructures. Previous work on this subject can be broadly classified into three categories, namely theoretical methods [7–9], experimental measurements [10,11] and computational simulations [12–22]. Because of the complex microstructure of the IPCs, an analytical method can hardly estimate the mechanical properties precisely. And experiment tests are inconvenient and costly. Hence, computational simulation methods are always employed and documented in literature. With 2D mesoscopic model using the Voronoi tessellation technique, Wang et al. [12] performed FE analysis on the representative volume element to study the mechanical properties of IPC. Singh et al. [13,14] presented a 2D unit cell model to numerically simulate the elastoplastic behavior of IPC using the element free Galerkin method (EFGM). Senthil et al. [15,16] used the random morphology description functions (RMDFs) to generate a so-called realistic random microstructure (2D) for computational analyses. Chen et al. [17] developed a routine for creating 2D FE models characterizing the microstructure observed in a SEM using a backscattering detector. However, a 2D model can hardly characterize IPCs exactly, whose constituents are interconnected in 3D space instead of scatter. Tuchinskii [9] presented a skeletal structure to estimate the elastic constants of pseudoalloys by theoretical analysis method. Feng et al. [7,8] presented a micromechanical model to estimate the effective elastic moduli of IPC by theoretical analysis method and finite element method. Furthermore, the elastoplastic behavior was derived via a step-by-step analysis of the unit cell. Jhaver and Tippur [3] presented a Kelvin cell based 3D elastoplastic finite element model capable of capturing both linear and nonlinear characteristics of the IPC foams. Nevertheless, these micromechanical models are far different from the realistic microstructure of IPC. To approach the realistic microstructure, Alveen et al. [18] presented a representative finite volume (FV) microstructure using Voronoi tessellation to synthetically represent the microstructure of a two phase ceramic composite. Poniznik et al. [19] established a random voxel model by FEM to estimate the effective elastic properties of metal-ceramic interpenetrating phase composites, and a

* Corresponding author. Tel.: +86 10 82315707; fax: +86 10 82318501.
E-mail address: luzixing@buaa.edu.cn (Z. Lu).

http://dx.doi.org/10.1016/j.commatsci.2014.10.021
0927-0256/

realistic microstructure FE model was introduced by contrast. These two FE models were much more approximated to the realistic structure of the materials compared to Tuchinskii's model [9], Feng's model [7,8] and Jhaver's model [3]. Basista et al. [20] developed a computational model to determine the Young modulus of IPC using 3D images of realistic material microstructure obtained from X-ray tomography. Nonetheless, obtaining the FE model based on a realistic microstructure is complex and expensive, which demands equipment severely. Except mesh-free method and FEM, molecular dynamics simulations (MDs) are also employed to study nano-IPCs. Yang and Lu [21] investigated the mechanical behavior of co-continuous Cu/SiC nanocomposites by MDs. They concluded that both the volume fraction (VF) of the components and temperature could affect the mechanical properties. Sun et al. [22] summarized four models to discuss the tensile property of IPC by MDs. It was concluded that the connectivity of microstructure in a certain direction strongly affects the effective Young's modulus and strengths of nanocomposites in this direction.

The interpenetrating metal-ceramic and pseudo-alloy are advanced engineering materials which have extensive applications. The fabrication of these IPCs always involves two steps, one of which is to prepare an interconnected porous structure, and the other is to infiltrate the molten phase into the porous structure [23,24]. In order to better predict material behavior, it is a key problem to establish a model which can describe the realistic microstructure of porous structure with co-continuous structure. Chen and Shen [25] characterized a co-continuous structure via solving the phase field equation and obtained realistic morphology. Inspired by the previous work, a realistic morphology is introduced into FEM and a random 3D FE model is presented to characterize the IPCs based on the phase field method for the first time.

The objective of this paper is to study the mechanical behavior of IPCs and the organization is as follows. First, the FE models (random, cross-cubic and tetrakaidecahedron models) are presented in detail. Next, the statistical and error analyses are introduced to determine the optimized random model parameters. Afterward, the optimized model is employed to predict the elastic and elasto-plastic properties of IPCs. The influences of the constituents' material parameters on the mechanical behaviors are also analyzed.

2. Models

2.1. Random model

IPCs have a complicated bicontinuous microstructure (Fig. 1) as their processing methods include direct porous structure and another phase infiltration into the matrix. To better mimic this process, a random porous model should be built at first, and then fill the porous model with another phase to obtain the whole IPC model. The phase field method has been usually employed to characterize the bicontinuous structures [22,26–29]. Sun et al. [22] established a bicontinuous structure based on the phase field method and MDs was implemented to obtain the mechanical behaviors of nano-IPC. Crowson et al. [26,27] probed the dominant mechanisms for the geometric relaxation of bicontinuous nanoporous metal based on the phase field method. Farkas et al. [28] and Sun et al. [29] studied the mechanical properties of nanoporous gold with bicontinuous structure based on the phase field method. As Section 1 mentioned, the existing FE models are either too simple to characterize the IPCs, or so expensive to obtain based on X-ray CT scan. Consequently, we utilize the phase field method to obtain the model information and implement FEM to establish model.

In the phase field method, the pattern evolution can be described by the Cahn–Hilliard equation [30]. The Cahn–Hilliard equation has a rather broad range of application. It can serve as a good model for the dynamics in a sufficiently accurate fashion so that many of the various features of the resultant pattern formation evolution during phase separation can be explained and predicted. As mentioned in Ref. [30], this pattern formation is referred to as the microstructure of the material in materials science. Consequently, a random bicontinuous structure pattern can be obtained by the following Cahn–Hilliard equation.

$$u_t = \nabla \cdot \left\{ M(u) \nabla \left[\frac{df(u)}{du} - \eth^2 \Delta u \right] \right\}, \tag{1}$$

where $u(x, y, z, t)$ is the difference in concentration of the two phases, t represents the evolutionary time, u_t denotes the partial time derivative of u, $f(u)$ is a free energy function, $M(u)$ is a "mobility" coefficient, $0 > \eth^2 \ll 1$ is a "coefficient of gradient energy", $\eth$ denotes the width of transition region between the two phases. In this study, we simply adopt the double-well potential function $f(u) = \frac{1}{4}(u^2 - 1)^2$, and consider $M(u)$ as a constant coefficient 1 and set $\eth = 0.01$ which does not influence the results qualitatively. We adopt the central difference method to discretize Eq. (1). A set of initial values are randomly generated near zero, and periodic boundary conditions are adopted in all three directions. The size of computational domain determines model size, which can be adjusted as needed.

We set a cutoff value u_0 to distinguish different phases. If $u \geq u_0$, the coordinate position is occupied by one phase, otherwise the coordinate position is the other phase. We can change the value of u_0 to obtain various VFs of constituents. Indeed, different random models can be obtained at different evolution time.

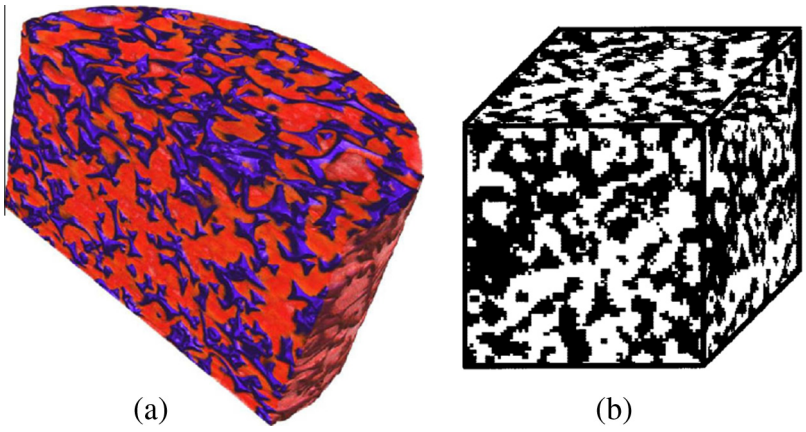

Fig. 1. (a) Microstructure of Al_2O_3–Cu composite, X-ray CT scan [19]. Reused with permission from ref. [19]. Copyright 2008 Elsevier. (b) Schematic of an interpenetrating two-phase composite [38]. Reused with permission from ref. [38]. Copyright 2004 John Wiley and Sons.

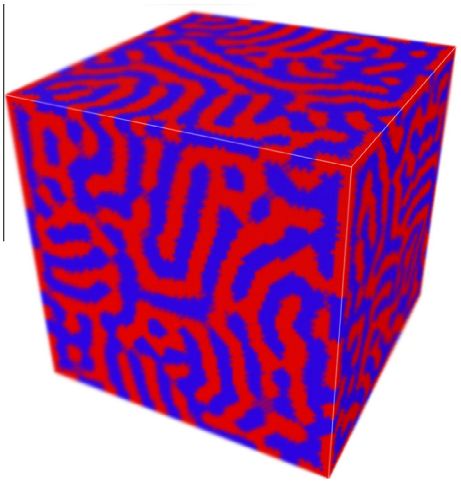

Fig. 2. Schematic of an IPC based on the phase field method (50% VF).

Fig. 2 is a schematic of an IPC (50% VF) based on the phase field method, which is geometrically periodic in all dimensions.

After collecting the information of coordinate position, a routine is compiled and FEM is implemented. We displace the coordinate position with a set of voxels (8-node elements in this study) and give them different material properties. The interface between two phases is considered as perfect interface. In conclusion, a random interpenetrating FEM model is achieved, as shown in Fig. 3(a).

2.2. Cross-cubic model

A cross-cubic model was used to study IPCs in earlier work [7–9]. Here, we also adopt this simple analytical model, as shown in Fig. 3(b). With the assumption of macroscopically homogeneous and isotropic materials, the cross-cubic unit cell can be divided according to the iso-strain and iso-stress assumption in two different ways. The lower and upper bound for the effective Young's modulus of IPCs with two constituents can be estimated as [21]

$$E_{eff}^{low} = f_1^2 E_1 + f_2^2 E_2 + 2 f_1 f_2 (f_1/E_1 + f_2/E_2)^{-1}, \tag{2}$$

$$E_{eff}^{up} = \left[\frac{f_2}{f_1^2 E_1 + \left(1 - f_1^2\right) E_2} + \frac{f_1}{f_2^2 E_2 + \left(1 - f_2^2\right) E_1} \right]^{-1}, \tag{3}$$

where E_1 and E_2 are the Young's modulus of each constituents, respectively. f_1 is the edge length as shown in Fig. 3(b) and $f_2 = 1 - f_1$.

2.3. Tetrakaidecahedron model

The tetrakaidecahedron consists of eight hexagon faces and six quadrilateral faces, in which every edge has the same length. Tetrakaidecahedron model, or Kelvin model was generally applied to study low-density open-cell foam [31,32]. Moreover, Jhaver and Tippur [3] and Tippur and Periasamy [33] developed a Kelvin cell based 3D elastoplastic finite element model and examined the feasibility of predicting both the elastic and plastic characteristics of the IPC foam. Similarly, we suppose that the tetrakaidecahedron has a uniform circle cross section of every ligament with the round joints. A cubic unit cell is built by filling the space of tetrakaidecahedron and 3-D tetrahedral solid element is adopted in ANSYS software to guarantee the compatibility between elements, as shown in Fig. 3(c). We can obtain various models with different VFs of components by changing the value of ligament radius.

2.4. Boundary conditions

The above three FE models are all geometrically periodic, so periodic boundary conditions [34] (PBC) are adopted in this study to ensure the continuity of forces and displacements on the opposite faces of the model.

3. Model analysis

Due to the structural randomness apparent in the FE model, the statistical and error analyses of the calculated results are significant. Based on our previous work [35,36], we discuss the effects caused by the model size, mesh sensitivity and the sample capacity. The following discussions are based on the results calculated with the parameters from the existing literatures [12,37], as shown in Table 1.

3.1. Model size and mesh sensitivity

To a random model, the effect of model size can be extremely crucial. The results based on a random FE model with small size exhibit far too much scatter to draw definitive conclusions regarding the macroscopic properties. However, the computational cost becomes prohibitive when the size is too large. Consequently, a suitable model size is crucial for our simulation. To facilitate comparison, the same VF of either constituent is chosen.

The number of meshes increases as the size of model increases, which can be indicated as mentioned in Section 2. Therefore, a FE model with an appropriate size is related to the number of meshes, which becomes a critical FE model for simulation in this study.

Fig. 4 reveals the influences of model size on Young's modulus with different VFs of constituent. The values decrease as the model size increases. The discrepancy of the mean Young's modulus between the $20 * 20 * 20$ model and the $45 * 45 * 45$ model is 3.84%, 4.30% and 4.87% for the VF of 32%, 35% and 39%, respectively. When the model size reaches 40∗40∗40, the calculated results become insensitive to the model size. Furthermore, the discrepancy of the mean Young's modulus between the $40 * 40 * 40$ model and the $45 * 45 * 45$ model is 0.11%, 0.51% and 0.14%, respectively.

According to the obtained data, we conclude that the critical model size is $40 * 40 * 40$. These dimensions balance the computational precision and efficiency, and we adopt this model to complete the following simulation.

3.2. Sample capacity

For our random FE model, the mean values from different models are generally used to estimate the effective mechanical properties. Evidently, more precise results would be obtained as the sample capacity (amount of models) increases. However, much sample capacity would cost much computational time. Hence, an appropriate sample capacity is selected in a statistical approach. The convergent relative error of mean value (REMV) and relative standard deviation (RSD) are determined as follows, respectively [35].

$$REMV = \frac{|M_{n+1} - M_n|}{M_{n+1}} \times 100\%, \; M_n = \frac{\sum_{i=1}^{n} Q_i}{n}, \tag{4}$$

$$RSD = \frac{D_n}{M_n}, \quad D_n = \sqrt{\frac{\sum_{i=1}^{n} (Q_i - M_n)^2}{n}} \tag{5}$$

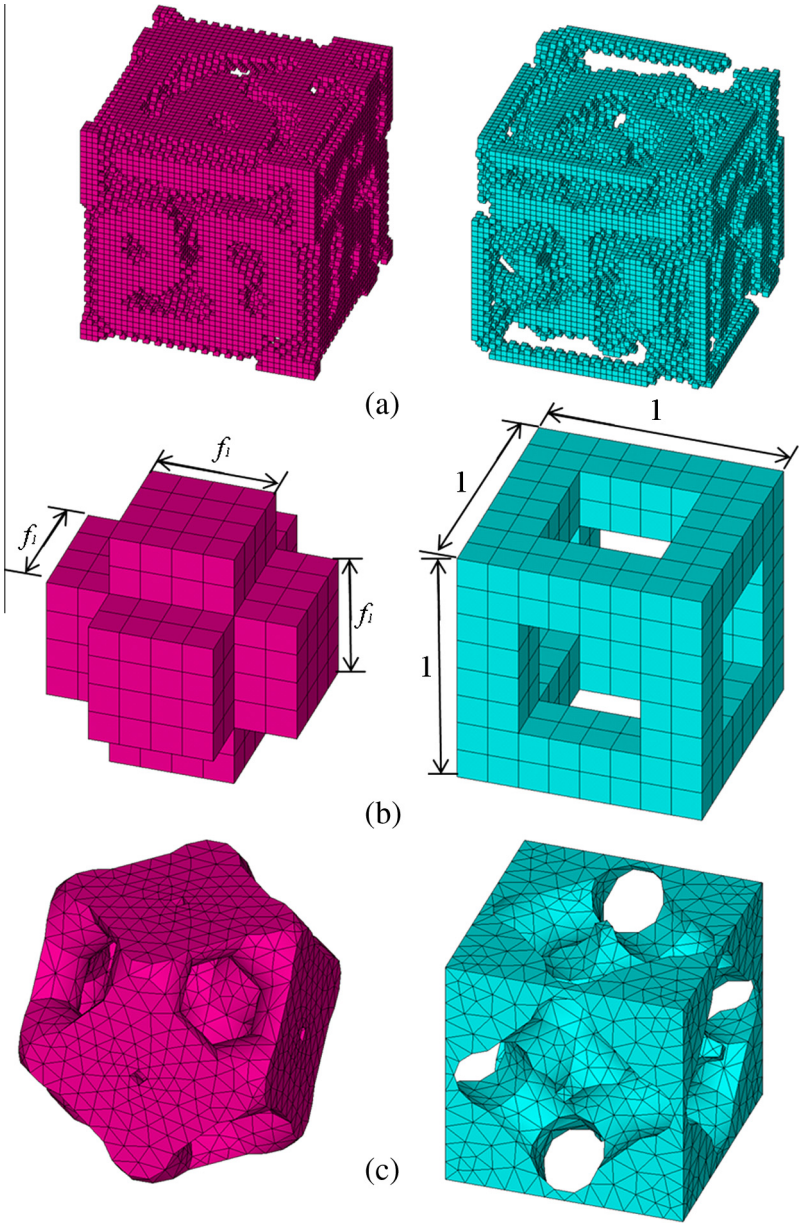

Fig. 3. FE models of (a) random, (b) cross-cubic and (c) tetrakaidecahedron.

Table 1
Summary of parameters used in the FE models.

	Young's modulus E (GPa)	Poisson's ratio v	Yield stress σ_y (MPa)	Tangent stiffness T (GPa)
Al_2O_3[a,b]	390	0.2	–	–
$AlSi_{12}$[a]	73	0.33	–	–
Epoxy[b]	3.4	0.35	–	–
Tungsten[c]	410	0.28	1200	14.5
Copper[c]	110	0.345	57	–

[a] From the literature [37].
[b] From the literature [6].
[c] From the literature [12].

where Q_i is the value obtained from numerical sample i, M_n and D_n are the mean values and standard deviations calculated using n numerical samples, respectively.

To facilitate comparisons, the model size $(40 * 40 * 40)$ and mesh density of these FE models are fixed when the influences of sample capacity are discussed. As shown in Fig. 5, we calculate the REMVs and RSDs for E and σ_y values, respectively. It is evident that the REMVs and RSDs both decrease when the sample capacity increases. Fig. 5(a) illustrates that the REMVs are below 1% since the sample capacity exceeds five. The convergence rate for each RSD is as quick as the corresponding REMV, as displayed in Fig. 5(b). The RSDs are below 1% since the sample capacity exceeds three and are below 0.5% when the sample capacity reaches five. Therefore, the following simulations adopt the mean values of five samples for each parameter.

4. Results and discussion

Based on the above discussions, the $40 * 40 * 40$ model is chosen as the critical size model. Hence, this model is adopted for the following simulations and all parameters are determined by averaging five samples.

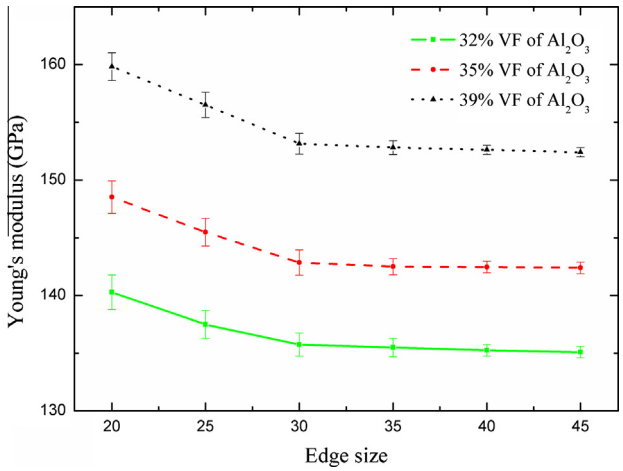

Fig. 4. The influence of model size on Young's modulus.

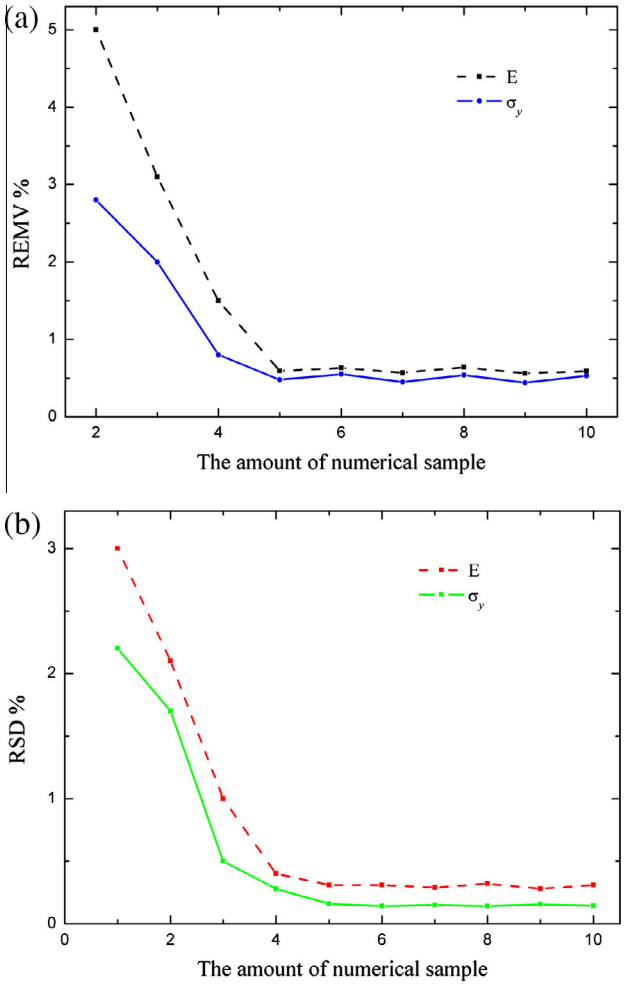

Fig. 5. The convergence of the (a) REMVs and (b) RSDs of the effective mechanical properties.

4.1. Elastic properties

The effective Young's moduli have been calculated and compared by using different analytical and numerical methods. The microstructures of the composites are either determined by the phase field method as mentioned above, or using previous cross-cubic model and tetrakaidecahedron model. The parameters of constituents are listed in Table 1.

Fig. 6 illustrates the effective Young's modulus of IPC versus the VF of Al_2O_3 which increase nonlinearly as the VF of Al_2O_3 increase. The FEM calculations for random microstructure, cross-cubic and tetrakaidecahedron are compared with the analytical low bound and up bound which are expressed as Eqs. (2) and (3). Blocks and spots represent the experimental data from previous literature [6,37]. It is observed that the analytical low bound and up bound cannot cover the experimental data completely. Due to real microstructure imperfections (e.g. microcracks, voids, etc), the experimental measurements may have values falling below the analytical low bound. The results of the cross-cubic model and tetrakaidecahedron model are both higher than the experimental data, but the results of the random model fit the experimental data well for two kinds of IPCs. The reason is that the morphology of the cross-cubic model and tetrakaidecahedron model is far more different from the realistic microstructure of IPC. However, the random model in this study can characterize this microstructure to a certain extent. It is also revealed that the random model can characterize the IPC based on different material system.

4.2. Elastoplastic properties

To study the elastoplastic properties of IPC, we assume that the constituents of IPC obey the elastoplastic constitutive relations. In this study, a set of parameters are chosen to simulate the elastoplastic behaviors of IPC, as listed in Table 1. Based on the literature [12], the stress–strain relationship of tungsten is supposed as a bilinear relationship. And the stress–strain relationship of copper

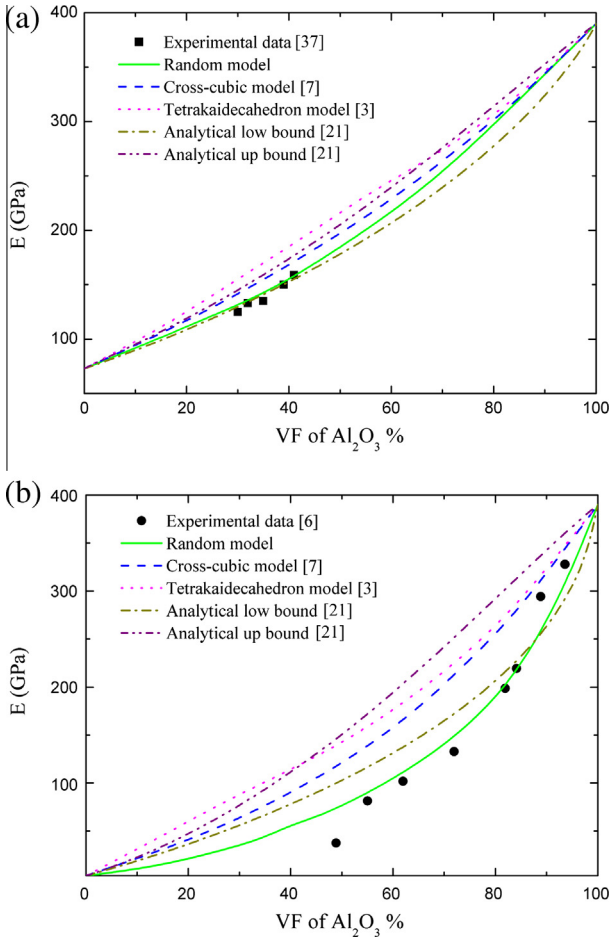

Fig. 6. Comparison with FEA results and the experimental data (a) for Al_2O_3–$AlSi_{12}$ and (b) for Al_2O_3–Epoxy.

is obtained by experimental data in the literature. The VFs of copper and tungsten are obtained through the density of CuW 70 wt.%, namely 48% and 52%, respectively. As shown in Fig. 7, the tensile stress–strain curves of different FE models are exhibited when the VF of copper is chosen as 48%, and the stress–strain relationships of two constituents are also presented. It is observed that there is an increase in modulus and strength of composite by addition of hard reinforcement. The curves of the cross-cubic model and tetrakaidecahedron model are close with each other and higher than the curve of the random model. The Young's modulus predicted by the cross-cubic model and tetrakaidecahedron model are also higher than that predicted by random model, which are determined by the initial slopes of the curves. According to the conventional definition, the yield stress is determined at 0.2% residual plastic strain (0.2% offset yield strength σ_y), and the yield strain is determined at the same position. A comparison of them is presented in Fig. 8. The yield stresses predicted by the cross-cubic model and tetrakaidecahedron model are higher than that predicted by the random model, which has a similar tendency with Young's modulus. However, there is only a little difference for yield stress between the cross-cubic model and tetrakaidecahedron model. The yield strain predicted by the cross-cubic model is just lower than that predicted by the random model, and both of them are observably lower than that predicted by the tetrakaidecahedron model.

Fig. 9(a) displays the stress–strain curves of various VFs of copper (%) predicted by the random model, which rise as the VF of copper decreases. The modulus and strength of tungsten are much higher than those of copper, so the influence of the VF of tungsten is significant. Fig. 9(b) shows the yield stresses for different FE models versus the VF of constituents. From this plot, it is observed that all the FE predicted values decrease nonlinearly as the VF of copper increases. It is found that different microstructures strongly affect the yield stress of IPCs. The yield stresses predicted by the cross-cubic model and tetrakaidecahedron model are close. The yield stresses predicted by random model are obviously lower than the others and closer to the experimental data. Hence, the random FE model is proved to be better utilized to describe the elastoplastic behaviors of IPC.

The stress–strain relationships of constituents have a great influence on the behavior of IPC, which is mainly governed by some parameters, like initial stiffness, yield stress and tangent stiffness. These parameters can change the nature of the resultant behavior of the IPC. Afterwards, the influences of various parameters are discussed when the VF of each phase is 50%. Fig. 10 shows the different stress–strain curves for the different values of yield

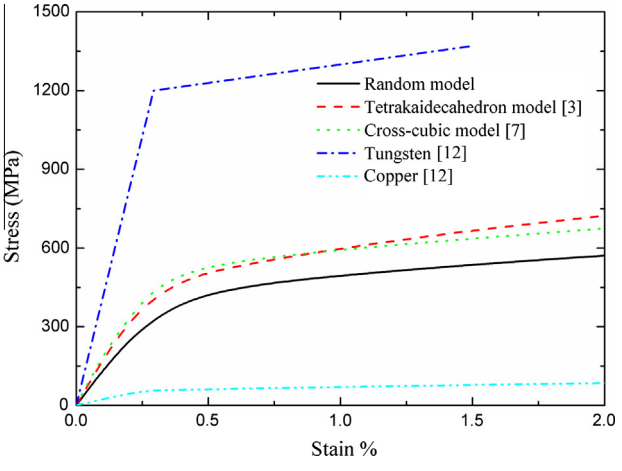

Fig. 7. Stress–strain curves predicted by different FE models.

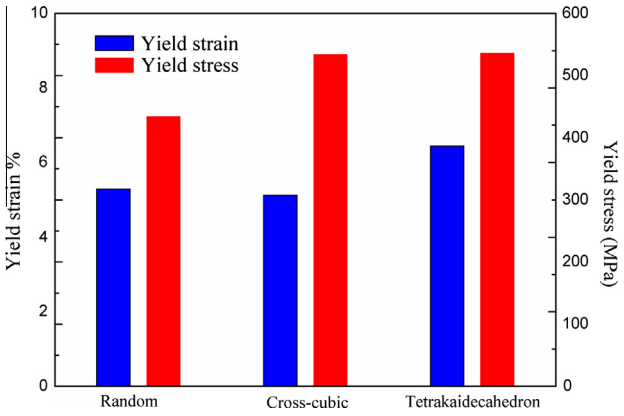

Fig. 8. Yield stress and yield strain predicted by different FE models.

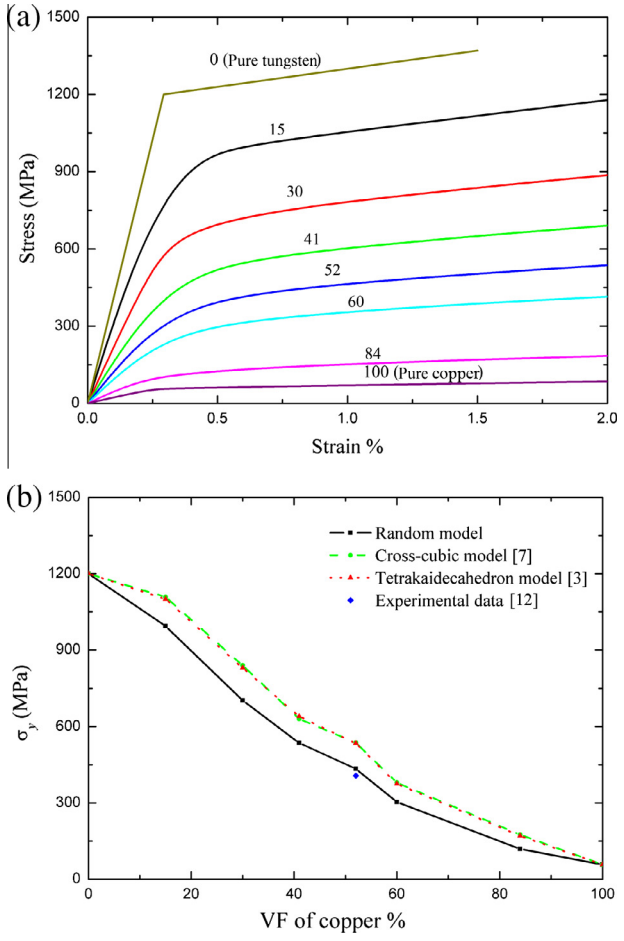

Fig. 9. (a) Comparison of stress–strain curve for different VFs of copper predicted by random model and (b) yield stress predicted by different FE models.

stress in hard phase with all other material constants unchanged. It is observed that the yield stress in hard phase has little effect on initial stiffness and yield stress. However, the plateau stress increases as the yield stress in hard phase increases. Fig. 11 displays the different stress–strain curves for the different values of yield stress in soft phase with all other material constants unchanged. It is observed that the initial stiffness, yield stress and plateau stress all increase as the yield stress in soft phase increase. Fig. 12 shows the different stress–strain curves for the different values of tangent stiffness in hard phase with all other material constants unchanged. The tangent stiffness in hard phase

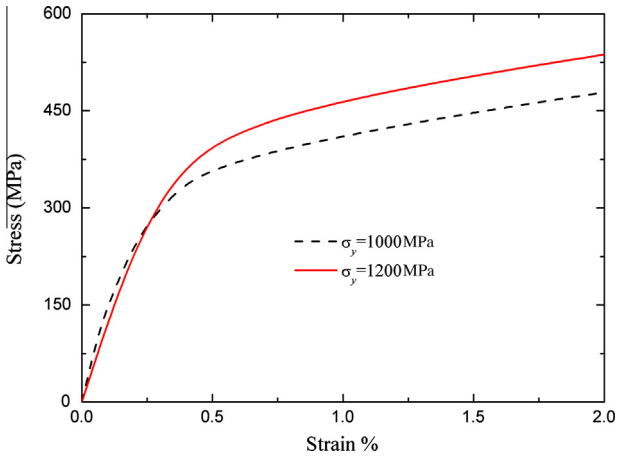

Fig. 10. Behavior of IPC for different material properties (σ_y) in hard phase.

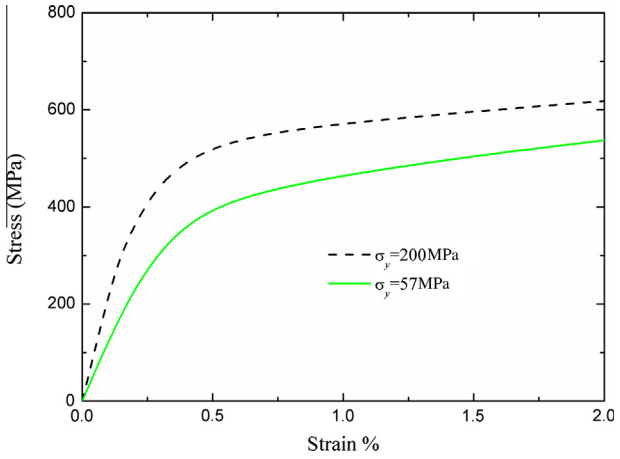

Fig. 11. Behavior of IPC for different material properties (σ_y) in soft phase.

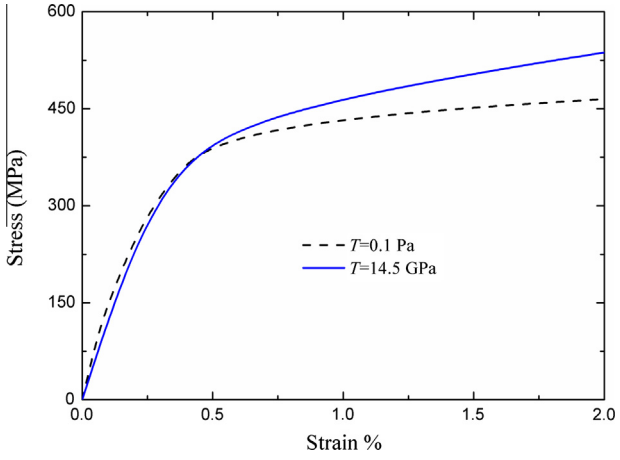

Fig. 12. Behavior of IPC for different material properties (T) in hard phase.

has almost no effect on initial stiffness and yield stress, but the plateau stress decreases a little. The most sensitive parameter is the yield stress in soft phase, for which a small change affects the overall behavior of IPC by large extent. Hence, the elastoplastic behavior of IPC depends on the yield stress in soft phase primarily.

5. Conclusions

A solving process to the phase field equation has been used to describe the spatial distributions of interpenetrating phases. A routine has been compiled and a 3D random FE model based on the phase field method has been presented to characterize the realistic microstructure of IPC for the first time. Inspired by previous work [3,7–9], the cross-cubic model and tetrakaidecahedron model are also conducted by FEM for comparison.

The statistical criterion has been employed to determine the critical size of the 3D random FE model. The sample capacity for REMVs and RSDs has also been discussed. The conclusion of the critical size being $40 * 40 * 40$ has been obtained.

After that, the 3D random FE model has been employed to predict the elastic and elastoplastic behavior of IPC. The predicted results of the cross-cubic model and tetrakaidecahedron model are also displayed for comparison. It is observed that the predicted results by the 3D random FE model accord better with the experimental data because of its realistic morphology.

In the present work, the 3D random FE model is only employed to predict the elastic and elastoplastic behavior, but it has the potential to predict the progression of damage using a continuum damage approach because of its realistic structure. Moreover, this simulation method offers the potential to model additional features of the real material, such as porosity, anisotropy and residual stress due to microcracking or debonding between phases.

Acknowledgements

The authors thank the support from the National Natural Science Foundation of China (11472025, 11272030 and 10932001).

References

[1] S. Roy, J. Gibmeier, V. Kostov, et al., Acta Mater. 59 (4) (2011) 1424–1435.
[2] X. Zhao, J. Mech. Phys. Solids 60 (2) (2012) 319–332.
[3] R. Jhaver, H. Tippur, Mater. Sci. Eng.: A 499 (1) (2009) 507–517.
[4] C. Periasamy, R. Jhaver, H.V. Tippur, Mater. Sci. Eng.: A 527 (12) (2010) 2845–2856.
[5] L. Zhao, M. Zhao, N. Li, et al., T. Nonferr. Metal. Soc. 20 (2010) s463–s466.
[6] M.T. Tilbrook, R.J. Moon, M. Hoffman, Mater. Sci. Eng.: A 393 (1) (2005) 170–178.
[7] X. Feng, Y. Mai, Q. Qin, Compd. Mater. Sci. 28 (3) (2003) 486–493.
[8] X. Feng, Z. Tian, Y. Liu, et al., Appl. Compos. Mater. 11 (1) (2004) 33–55.
[9] L.I. Tuchinskii, Powder Metall. Met. C+ 22 (7) (1983) 588–595.
[10] B. Commentz, C. Hartig, H. Mecking, Compd. Mater. Sci. 16 (1) (1999) 237–247.
[11] L.D. Wegner, L.J. Gibson, Int. J. Mech. Sci. 42 (5) (2000) 925–942.
[12] Y. Wang, S. Liang, P. Xiao, et al., Compd. Mater. Sci. 50 (12) (2011) 3450–3454.
[13] A. Agarwal, I.V. Singh, B.K. Mishra, J. Compos. Mater. 47 (11) (2013) 1407–1423.
[14] A. Agarwal, I.V. Singh, B.K. Mishra, Compos. Part B: Eng. 51 (2013) 327–336.
[15] S.S. Vel, A.J. Goupee, Compd. Mater. Sci. 48 (1) (2010) 22–38.
[16] A.J. Goupee, S.S. Vel, Compd. Mater. Sci. 48 (1) (2010) 39–53.
[17] G. Chen, U.A. Ozden, A. Bezold, et al., Compd. Mater. Sci. 80 (2013) 96–103.
[18] P. Alveen, D. Carolan, D. McNamara, N. Murphy, A. Ivanković, Compd. Mater. Sci. 79 (2013) 960–970.
[19] Z. Poniznik, V. Salit, M. Basista, D. Gross, Compd. Mater. Sci. 44 (2) (2008) 813–820.
[20] W. Węglewski, K. Bochenek, M. Basista, et al., Compd. Mater. Sci. 77 (2013) 19–30.
[21] Z. Yang, Z. Lu, Compos. Part B: Eng. 44 (1) (2013) 453–457.
[22] X. Sun, Q. Li, Y. Gu, X. Feng, Compd. Mater. Sci. (2013).
[23] X. Wang, P. Zhang, L.H. Dong, et al., Mater. Design 54 (2014) 995–1001.
[24] H.M. Fu, N. Liu, A.M. Wang, et al., Mater. Design (2014) 182–186.
[25] L.Q. Chen, J. Shen, Comput. Phys. Commun. 108 (2) (1998) 147–158.
[26] D.A. Crowson, D. Farkas, S.G. Corcoran, Scripta Mater. 56 (11) (2007) 919–922.
[27] D.A. Crowson, D. Farkas, S.G. Corcoran, Scripta Mater. 61 (5) (2009) 497–499.
[28] D. Farkas, A. Caro, E. Bringa, et al., Acta Mater. 61 (9) (2013) 3249–3256.
[29] X. Sun, G. Xu, X. Li, et al., J. Appl. Phys. 113 (2) (2013) 23505.
[30] A. Novick-Cohen, Handbook Differen. Equat.: Evolutionary Equat. 4 (2008) 201–228.
[31] H.X. Zhu, J.F. Knott, N.J. Mills, J. Mech. Phys. Solids 45 (3) (1997) 319–343.

[32] Z. Lu, C. Zhang, Q. Liu, et al., J. Phys. D: Appl. Phys. 44 (39) (2011) 395404.
[33] C. Periasamy, H.V. Tippur, Mech. Res. Commun. 43 (2012) 57–65.
[34] Z. Lu, B. Xia, Z. Yang, Compd. Mater. Sci. 77 (2013) 445–455.
[35] Q. Liu, Z. Lu, Z. Hu, et al., Mater. Sci. Eng.: A 587 (2013) 36–45.
[36] Q. Liu, Z. Lu, M. Zhu, et al., J. Mater. Sci. 49 (3) (2014) 1386–1398.
[37] R.J. Moon, M. Tilbrook, M. Hoffman, et al., J. Am. Ceram. Soc. 88 (3) (2005) 666–674.
[38] S. Torquato, C.L. Yeong, M.D. Rintoul, et al., J. Am. Ceram. Soc. 82 (5) (1999) 1263–1268.